Title

Substantial potential effects on single-atom catalysts for the oxygen evolution reaction simulated via a fixed-potential method

Authors

Gao, Guoping
Wang, Lin-Wang

Publication Date

2020-11-01

DOI

10.1016/j.jcat.2020.08.032

Peer reviewed

Volume 390, October 2020

ISSN 0021-9517

JOURNAL OF CATALYSIS

Available online at www.sciencedirect.com

ScienceDirect

Journal of Catalysis 391 (2020) 530–538

Contents lists available at ScienceDirect

Journal of Catalysis

journal homepage: www.elsevier.com/locate/jcat

Substantial potential effects on single-atom catalysts for the oxygen evolution reaction simulated via a fixed-potential method

Guoping Gao *, Lin-Wang Wang

Materials Sciences Division, Lawrence Berkeley National Laboratory, Berkeley CA 94720, United States

ARTICLE INFO

Article history:
Received 30 July 2020
Revised 10 August 2020
Accepted 26 August 2020
Available online 12 September 2020

Keywords:
Oxygen evolution reaction
Fixed-potential method
Fixed-charge method
Electrical energy
Chemical energy

ABSTRACT

Potential not only governs the direction of electrochemical reactions, but also shapes the electronic properties of single-atom catalysts dramatically. However, it is a challenge to simulate the effects of potential theoretically. Normally, DFT calculations are performed at a constant number of electrons, not a constant voltage. In this work, we apply a new fixed-potential method (grand canonical method) in the DFT simulation to mimic the electrochemical processes, in which the total number of the electron in the system was floated to match the ''applied voltage,', or the electrode Fermi energy at the atomic level. Here, the single-atom catalysts on two-dimension substrates for the oxygen evolution reaction process are used as examples to test the fixed-potential method. This fixed-potential method changes the rate-determining step and yields an overpotential difference of as much as 0.48 V in comparison with the conventional charge-neutral method. The quantitative error in the overpotential is not as important as the qualitative error in rate-determining steps. These errors can be avoided via the fixed-charge method with the proper charge. We believe our work advances the understanding of the effects of potential on the catalytic process in real electrochemical reactions and offers practical guidance for designing catalysts.

1. Introduction

Electrochemical reactions, with interconversion of chemical energy and electrical energy, occur widely in metallurgy, electroplating, batteries, and water splitting. The applied voltage is crucial for these processes to occur. Obtaining the total free energy change (ΔG) of every elementary step under the applied voltage, including the electrical energy change (ΔG_{elect}) and chemical energy change (ΔG_{chem}), is vital for elucidating the underlying mechanism. So far, the common practice of DFT calculation to simulate electrochemical reactions is based on a constant number of electrons or constant charge state, not a constant voltage, which ignores the effects of potential on the reactivity in the experiment (grand canonical ensemble). The oxygen evolution reaction (OER), for example, which consumes the major energy in many electrochemical reactions, is the most important anodic reactions involving in energy conversion and storage processes, such as water splitting [1] and CO_2 reduction [2]. The widely-used four-charge-steps pathway model of OER was first proposed by Nørskov et al. to simulate the catalytic properties of pure metals and metal oxidation [3,4]. A computational hydrogen electrode (CHE) approach is proposed based on the idea that one electron will transfer from the charge-neutral system into the electrode reservoir in each elementary step. In this scheme (we named it the charge-neutral method (CNM)), it is only necessary to calculate the chemical formation energies ΔG_{chem} of *(bare substrate), OH*, O*, and OOH* intermediate species once at neutral charge and get the energy values of these intermediate states by adding the $N_e \times U$ term for any applied voltage U. More specifically, the U-dependent energy comes from $\Delta G_{elect} = N_e \times U$ only, where N_e is the number of electrons transferring in each step (e.g., N_e = 1 for each elementary step of OER). The thermodynamic overpotential η is derived from the minimum electrode potential U required to convert the above four steps exothermically. This CNM significantly reduces the cost of calculations [5,6]. However, the above calculation ignores the effects of U on the electronic properties of catalysts, or the U dependence of ΔG_{chem} and can introduce big errors, especially for low-dimensional catalysts, as we will show later. There are some modified models, such as the extrapolation scheme [7] and the double reference method [8], converting the reactivity calculated under the constant-charge condition to that under the constant-potential condition. However, these models require some extra experimental parameters and assumptions as benchmarks and are difficult to follow.

* Corresponding author.
E-mail addresses: ggp1234563344@gmail.com (G. Gao), lwwang@lbl.gov (L.-W. Wang).

https://doi.org/10.1016/j.jcat.2020.08.032
0021-9517/

Ideally, the reaction chemical energy under applied voltage should be calculated explicitly with constant U throughout the calculation. This approach will be a grand canonical calculation. In this approach, the electrode potential (Fermi energy) is fixed, while the total number of electrons can vary at the atomic level. A few prior works have applied this approach to investigate electrode potential effects. Head-Gordon et al. have proved that the potential effect changes the mechanism for C–C bond formation [9]. Liu et al. have shown that the charge effects of different potentials have a strong impact on the electrochemical reaction, especially in 2D materials [10]. However, the present grand canonical calculations are realized by adding an outside loop, which iterates the fixed-charge calculations through different charge values until the resulting Fermi energy reaches the desired value. Together with the requirement for the solvent model, this makes the grand canonical fixed-potential method (FPM) calculation rather expensive, and have only been used in limited cases so far. In the current work, a new computational approach, in which the orbital occupations in a self-consistent field (SCF) density functional theory (DFT) calculation are calculated using the fixed Fermi level [11], will be used to adjust the total charge of the system throughout the SCF iterations. In this implementation, a finite number is used at the $G = 0$ point, while $1/G^2$ is used at the other G point in the metrics during the Kerker preconditioning, and the Pulay charge mixing is not changed significantly. By doing so, one can change the orbital occupations. Note that one can use the auxiliary Hamiltonian method instead of this self-consistent field method [11]. We believe different codes favor different implementations. Based on our calculations, the self-consistent field method works fine. This direct grand canonical calculation, together with efficient implementation of the solvent model (including the linearized Poisson–Boltzmann equation), allows fast fixed-potential calculations. A proper expression for the total energy is required to obtain the variation minimum solution of the SCF procedure quickly. In addition, one can use the Hellman–Feynman force to guide molecular dynamics, atomic relaxation, and NEB calculations. All these functionalities work fine in the PWmat code.

Single-atom catalysts, for example those dispersing the transition metal atoms on 2D substrates, have emerged as a new research frontier for electrolytic water splitting, CO_2 reduction, NO_2 reduction, etc. [2,12–16]. The low-coordinated isolated transition metals in these catalysts usually exhibit excellent activity [17,18]. Meanwhile, these single-atom catalysts provide a relatively easy platform for theorists to explore the intrinsic reaction mechanisms due to their limited atomic configurations [6]. Combinations of different transition metals and substrates provide a large pool to deliver atomic-scale insight into the activity trends in a wide range of catalysts, allowing the designs of more effective and optimized catalysts [19]. The density of states of single-atom catalysts, especially for the transition metal d-states, is more susceptible to environmental conditions (such as potential, pH, charge states) than that of bulk or surface catalysts. At different U, the reaction site electronic structures (e.g., state occupation and charge state) will be different. That apparently will affect ΔG_{elect}, ΔG_{chem}, and the reaction mechanism. Here, we use transition-metal- and nitrogen-co-doped graphene (MN_4@graphene) and transition-metal-doped graphene (M@graphene) as examples to investigate the OER process via the FPM. In the FPM, the system is charged (not neutral) by accepting/donating electrons from/to the electrode to match the catalyst Fermi level with the applied electrode potential. The overpotentials obtained by the CNM and FPM can differ by as much as 0.48 V (NiN_4@graphene). The reaction-driving force caused by the increase of the electrode potential is greater in the FPM than in the traditional CNM. Based on the electronic properties of the M—O bond, we find that different electrode potentials give different local electronic structures and binding environments, which changes the catalytic activities and energies. Thus, one cannot use the local electronic structure at a neutral charge to describe the reaction at the operando electrode potential.

2. Computational details

All calculations were performed using the PWmat code [20,21] with norm-conserving SG15 pseudopotential. The PWmat is a plane wave pseudopotential package for density functional theory (DFT) calculations, which is designed to run efficiently on CPU/GPU processors by a drastic redesign of the algorithm and moving all the major computation parts into GPU. The exchange–correlation interactions are treated by the generalized gradient approximation in the form of the Perdew–Burke–Ernzerhof functional [22,23]. The electron wave functions are expanded by plane waves with cutoff energies of 680 eV, and the convergence tolerance for residual force and energy on each atom during structure relaxation are set to 0.005 eV $Å^{-1}$ and 10^{-5} eV, respectively. The van der Waals interaction is described using the empirical correction in Grimme's scheme, i.e., DFT + D_2 [24]. Here, we note that the hydrogen bonding from the local water is also important to electrochemical reactions [25]. However, it will make fixed-potential calculation much more challenging if some water molecules are included in our model. So the solid-water effect of the aqueous solution is approximated via the self-consistent continuum solvation model with a dielectric constant of 78 for both CNM and FPM calculations. Spin polarization is applied in all the calculations as well. The magnetic moment of the whole system or transition metal is calculated from the difference between spin-up and -down atomic charges based on the Hirshfield scheme. The Hubbard U (DFT + U) treatment is used on the transition metal. The U values for Co and Ni are set to 3.42 and 3.40, respectively, following the literature values [26].

The FPM, which can automatically adjust the total electrons of the system to satisfy an applied electrode potential [9,27], is implemented in the PWmat. Compared with fixed-charge (e.g., charge-neutral) calculations, the FPM could be more expensive. First, an implicit self-consistent continuum solvation model [28] together with a linearized Poisson–Boltzmann equation [29] must be used. The solvent model in PWmat is based on the framework of the self-consistent continuum solvation model [30], which is similar to the model used in VASPsol [28]. This solvation model uses a continuum mediate and a space variation dielectric constant $\varepsilon(r)$ to represent the solvation effects, mostly the polarization effects. The Poisson–Boltzmann equation is used to screen the effects of free ions, provide a reference potential (0 V) far away from the surface, and define the absolute potential of the electrode corresponding to the experimental potential in the fixed-potential (fixed-Fermi-energy) calculations. Second, in the previous literature, an outside loop in an existing ab initio package (e.g., VASP [10]) was used to adjust the total electron of the system until the desired Fermi energy is reached. In the current study, we have used the PWmat package, where a fixed-Fermi-energy self-consistent field (SCF) procedure was implemented in the DFT electronic structure calculation itself, so that it was not necessary to iterate through the outside loop to adjust the total electrons of the system. Overall, this has significantly speeded up the calculation. For a given U, compared with the normal fixed-charge calculation, the fixed-potential calculation is only about 50% more expensive. The PWmat code also allows atomic relaxation at a given constant potential U. The details of the computation for OER via the charge-neutral method can be found in the Supporting Information. The formulation of the fixed-potential method shown in the manuscript is based on these equations with proper modifications.

In this work, the electrode potential ($U_{\text{electrode}}$) or the electrode Fermi energy (E_F) used below is defined as the difference in elec-

tronic energy between a point outside the electrolyte in which the electrode is submerged (an electron at rest in the vacuum) and a point inside the metal (Fermi level) of an electrode, or the opposite values from absolute electrode potential, as illustrated in [31]. Also, note that $U_{electrode}$ = -(U_{NHE} + 4.40). Here, U_{NHE} refers to the normal hydrogen electrode (NHE) potential. The definition of electrode potential connects the "relative" electrode potential to the "absolute" physical quantities (Fermi level, E_F) of the calculated model. This vacuum reference potential is also the far-away potential from our Poisson–Boltzmann solution in our calculation. So the E_F used in our FPM is equivalent to the potential $U_{electrode}$ applied in the experiment.

3. Results and discussion

Fig. 1 presents the configurations of two types of single-atom catalysts made by dispersing transition metal atoms on 2D graphene-based substrates, transition-metal- and nitrogen-co-doped graphene (MN_4@graphene) and transition-metal-doped graphene (M@graphene), as studied in this work (M = Co or Ni). In MN_4@graphene, the single-atom transition metal is surrounded by four nitrogen atoms, while in M@graphene, it is surrounded directly by four carbon atoms. Both these two types are widely studied and realized in the experiment [13,14]. The low-coordinated isolated transition metals in these catalysts are considered as active sites due to their high activity.

The clean catalyst, OH*, O*, and OOH* (* denotes the catalyst) are considered as the four key stages of OER. Here, we choose CoN_4@graphene as an example to plot the DOS of these four stages via normal CNM (see left panel, Fig. 2) and FPM (see right panel, Fig. 2). In the CNM, the clean CoN_4@graphene's Fermi level is −3.88 eV. With intermediate species adsorbing, the Fermi level decreases to −4.27, −4.25, and −4.13 eV for OH*, O*, and OOH*, respectively. The variation in adsorbents tunes the Fermi level of the neutral catalyst to variable values. On the other hand, if we set the Fermi energy level to a constant value, −5.63 V (the ideal OER potential level) in the FPM, the total net charges of these four stages varied from + 1.25 to + 1.59e, which is far from zero. The charge varies as the reaction proceeds under fix Fermi level due to the oxidative state of transition metal changing during the process. The same phenomena are also confirmed by other catalysts as shown in Tables S1 and S2 in the Supporting Information. Also, the DOS of Co obtained in these two methods are dramatically different. Therefore, the CNM and FPM are performed under dramatically different local Fermi energies and orbital occupations, which create different microscopic environments for chemical reactions. The FPM directly follows the experimental conditions. Thus it should be more realistic.

In the following, we discuss how to use the FPM to calculate the Gibbs free energetics of the elementary steps in an OER process. The widely used four-charge-steps pathway model of OER via the charge-neutral method is summarized in the Supporting Information. Here, we take the first elementary charge step of OER as an example to compare the difference in the Gibbs free energy calculation between the CNM and FPM. Within the CNM, the first reaction can be written as

$$H_2O(l) + * - e^- \rightarrow OH^* + H^+ \quad (1)$$

In the CNM, the Gibbs free energy of this step (ΔG_{CNM}) is calculated as follows:

$$\Delta G_{CNM} = G_{OH^*} + \frac{1}{2}G_{H_2} + 4.4e - G_{H_2O(l)} - G_* - kT\ln 10 \cdot pH + eU_{electrode} \quad (2)$$

Here, an electron on the left-hand side is transferring from the surface/catalysis system to the electrode reservoir with Fermi energy at $U_{electrode}$. The lower the $U_{electrode}$, the smaller is the ΔG_{CNM}, and the more easily the reaction is realized. One can define the first five terms in Eq. (2) as chemical reaction formation energy: $\Delta G_{chem} = G_{OH^*} + \frac{1}{2}G_{H_2} + 4.4e - G_{H_2O} - G_* - kT\ln 10 \cdot pH$. Note that, in this CNM approximation, for every reaction step, the charge transfer from the surface/catalysis system (for which we calculated) to the electrode reservoir is always 1. Thus, one can define the electrical (or electronic) energy, the energy of an electron at rest in vacuum jumped down to the electrode potential: $\Delta G_{elect} = eU_{electrode}$. The total formation energy is thus the sum of the chemical reaction formation energy $\Delta G_{chem}$and the electrical energy ΔG_{elect}. As we can see, ΔG_{chem} and ΔG_{elect} are well defined by the above formulas and independent from each other in the CNM.

Under the FPM, the various intermediates' (OH*, O*, and OOH*) adsorption onto catalysts involves oxidative state changing in the transition metal at a constant potential, resulting in noninteger charge transfer. Assume that, before the reaction, the total charge is q_1, and after the reaction, the total charge is q_2; then the reaction equation that balances both the elements and charges should look like

$$H_2O(l) + *^{q_1} - (1 + q_2 - q_1)e^- \rightarrow OH^{*,q_2} + H^+ \quad (3)$$

(where q_1 and q_2 are defined as the positive charge determined by the $U_{electrode}$). In our FPM, what we calculated are the energies of $OH^{*,q_2}$and $*^{q_1}$. As a result, the reaction Gibbs free energy under FPM is

$$\Delta G_{FPM} = G^{q_2}_{OH^*} + \frac{1}{2}G_{H_2} + 4.4e - G_{H_2O(l)} - G^{q_1}_* - kT\ln 10 \cdot pH + (1 + q_2 - q_1)eU_{electrode}. \quad (4)$$

It is very interesting that in this elementary step, the charge flowing to the reservoir (e.g., the total current flowing through a wire connecting the electrode to the cathode) is not 1e ($q_1 \neq q_2$). Instead, it is (1 + q_2 - q_1)e. This charge is different for each step,

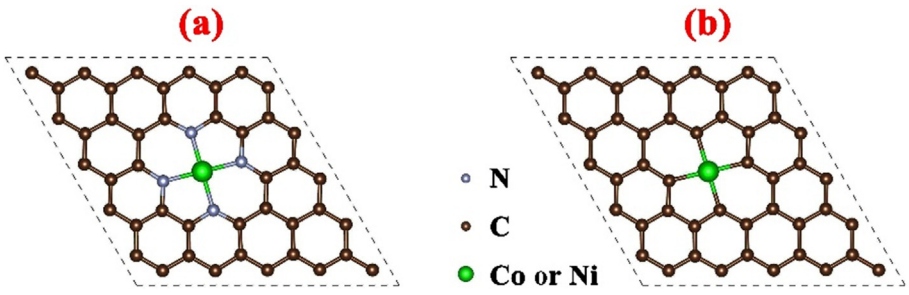

Fig. 1. The geometric structures of transition-metal- and nitrogen-co-doped graphene (MN_4@graphene, a), and transition-metal-doped graphene (M@graphene, b). M represents Co or Ni.

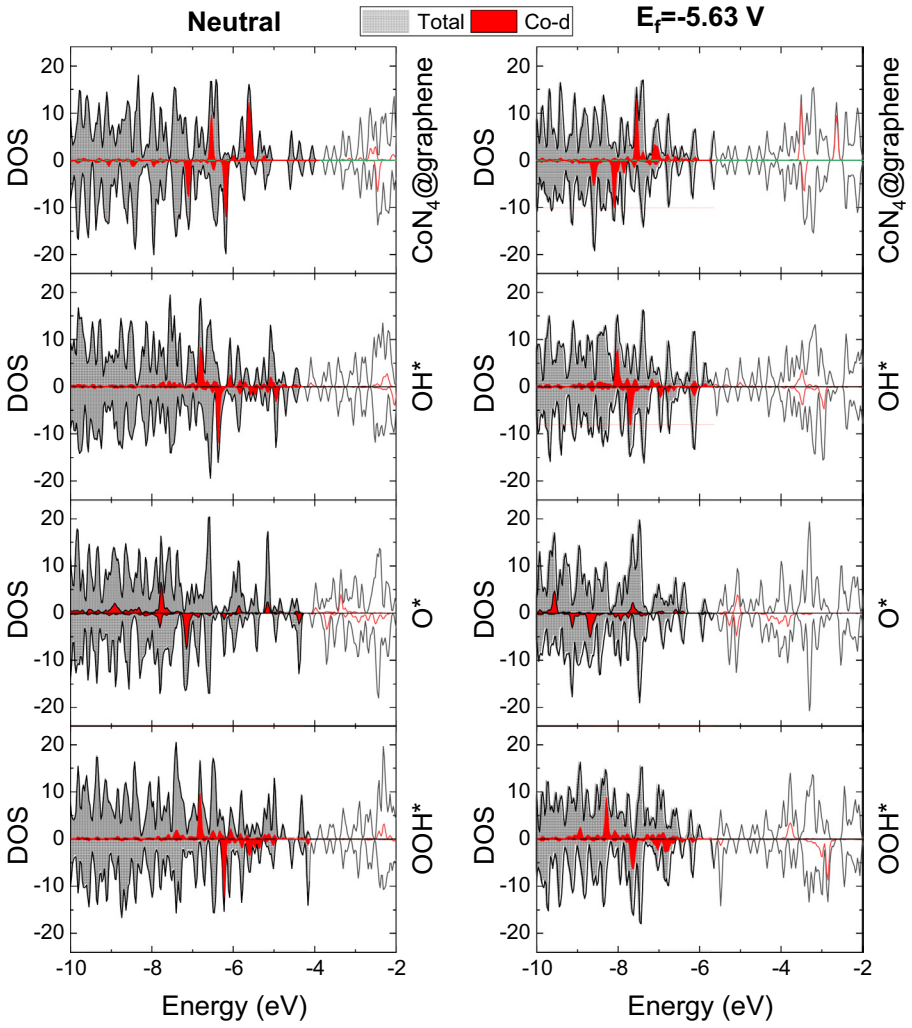

Fig. 2. The densities of state for CoN_4@graphene and CoN_4@graphene with OH*, O*, and OOH* adsorbing calculated by the normal charge-neutral method and the fixed-potential method (E_F = -5.63 V). In all the calculations, the vacuum energy levels are set to zero.

although the sum of the total charge for the four steps will remain 4*e*. This difference can certainly change the balance between different steps and the highest potential $U_{electrode}$ required to make all four steps exothermic. Following our definition in the CNM, ΔG_{chem} of this elementary step is obtained by $G^{q_2}_{OH*} + \frac{1}{2}G_{H_2} + e \times 4.4 - G_{H_2O(l)} - G^{q_1}_{*} - kT\ln 10 \cdot pH$, and the corresponding ΔG_{elect} is expressed by $+(1 + q_2 - q_1)eU_{electrode}$. Both terms are strongly dependent on $U_{electrode}$. Therefore, there is a strong correlation between ΔG_{chem} and ΔG_{elect}. In calculating $G^{q_2}_{OH*}$, we have included the contributions of vibrational entropy and vibrational zero-point energy. $G_{H_2O(l)}$is calculated by a vapor phase of water with low pressure that is in equilibrium with the liquid water. The gas-phase G_{H_2} at 1 atmosphere standard condition is calculated by its molecular energy plus the vibrational zero-point energy and vibrational entropy term (see the Supporting Information for more details).

Fig. 3 shows the free energy diagrams for OER of different single-atom catalysts obtained by the charge-neutral method and the fixed-potential method at different $U_{electrode}$. As the Fermi energy levels of neutral catalysts and their intermediate states in CNM are close to −4.4 V as shown in Table S1 in the Supporting Information, the energy paths obtained via the fixed-potential method (black solid line) are very close to those in the CNM (black dashed line), especially for the Co@graphene (Fig. 3b) and Ni@graphene (Fig. 3d) when $U_{electrode}$ = -4.4 V (the ideal SHE potential). In CNM, it is assumed that the intermediate energies at this $U_{electrode}$ correspond to the neutral charge results, However, in reality, two factors make the CNM and FPM different even at this *U*. First, in the FPM, the $U_{electrode}$ = -4.4 V does not correspond to the exact neutral charge system. From the bare surface * to all the intermediate states OH*, O*, OOH*, these systems are actually charged. Second, the charges for these systems under the FPM calculation are slightly different, which also causes energy differences between CNM and FPM at different intermediate states. In the FPM, q_2 - q_1 can still be rather large, e.g., −0.39*e* for the * to OH* step for CoN_4@graphene. The ΔG_{elect} obtained via CNM and FPM ((q_2 - q_1) $^*eU_{electrode}$) will give a 1.7-eV energy difference. There is no such large difference between FPM and CNM, as shown in Fig. 3a. Thus, the large electric energy ΔG_{elec} induced by this charge flow is compensated for by ΔG_{chem}.

When the potential decreases to $U_{electrode}$ = −5.63 V (the ideal oxygen evolution potential), a larger amount of electron charge in catalysts and their intermediates is donated to the reservoir of the electrode. As a result, the catalytic systems are more positively charged. This positive charge induces the different local orbital occupations between FPM and CNM, and different OER pathway curves. In reality, a potential lower than −5.63 V is required for any catalysts to drive the OER (overpotential). Since at $U_{electrode}$ =

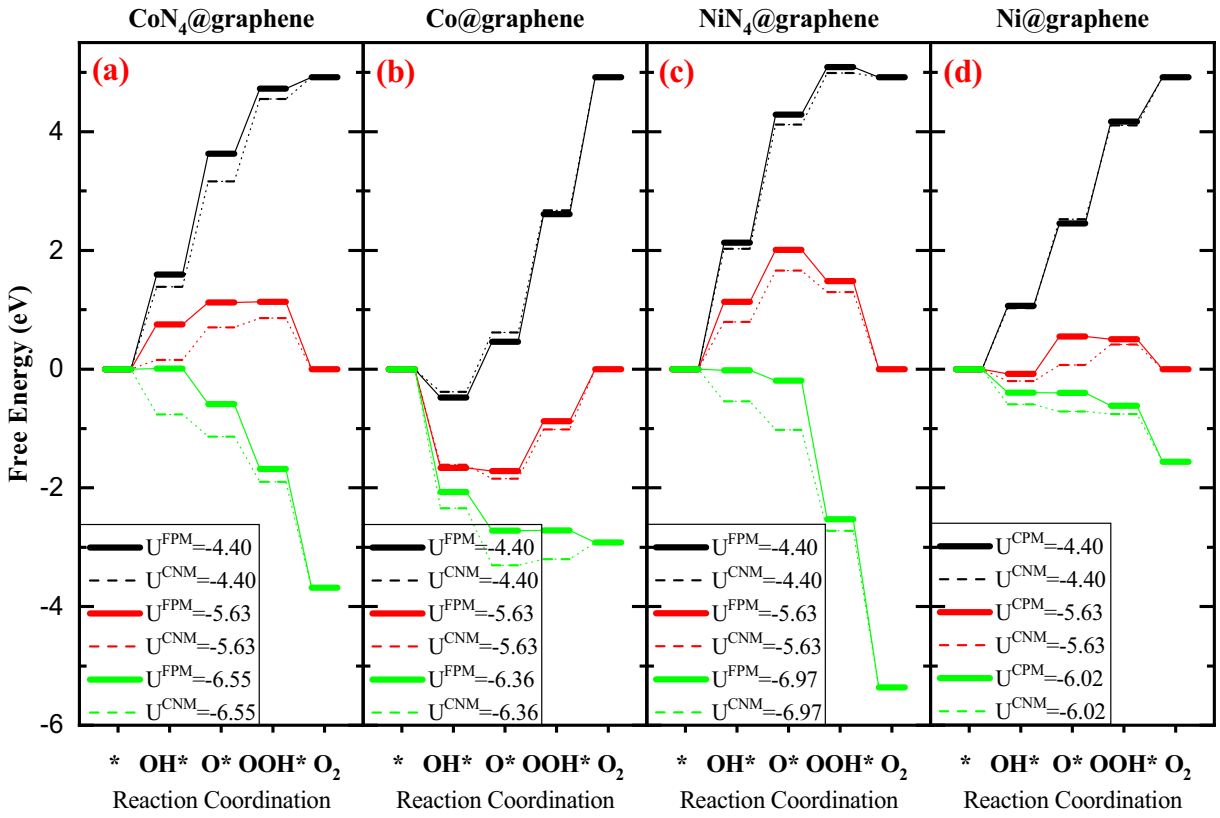

Fig. 3. The free energy diagrams for the oxygen evolution reaction on CoN_4@graphene(a), Co@graphene(b), NiN_4@graphene(c), and Ni@graphene(d). The results obtained by the fixed-potential method are plotted with solid lines, while the results obtained by the charge-neutral method are plotted with dashed lines. $U_{electrode}$ = -4.4 V is the ideal hydrogen evolution potential, while $U_{electrode}$ = -5.63 V is the ideal oxygen evolution potential.

−5.63 V, we already see a big difference between FPM and CNM curves, we expect these two methods to give an even bigger difference under the real working condition (see the green solid lines vs. the green dashed lines in Fig. 3). In the following, we analyze the errors in CNM in two aspects: the overpotential error and the energy error.

In the OER reaction, the thermal dynamic overpotential (η), in which we ignore the effect of kinetic barriers, is the most important parameter to evaluate the activities of catalysts. This overpotential allows us to estimate the reaction threshold (instead of the full Tafel plot). Computationally, the η can be calculated from the highest $U_{electrode}$ ($U^h_{electrode}$) which makes all four reaction steps exothermic:

$$\eta = -5.63 - U^h_{electrode} \quad (5)$$

Here, −5.63 eV is the theoretical ideal OER potential. In the CNM, the free energy dependence on $U_{electrode}$ is only based on the$\Delta G_{elect} = N_e{*}U_{electrode}$ term, as the ΔG_{chem} term is fixed. The $U^h_{electrode}$can be obtained relatively easily from the highest ΔG step in the $U_{electrode}$ = −4.4 plot via Eq. (8) in the Supporting Information. For FPM, one has to iterate the calculation with different $U_{electrode}$ until every elementary step is exothermic. In practice, when the $U_{electrode}$ is close to the $U^h_{electrode}$, one can assume the N_e is not changed and use the $\Delta G_{elect} = N_e{*}U_{electrode}$ to estimate the $U^h_{electrode}$. Thus, a few iterations will be sufficient to find $U^h_{electrode}$.

Table 1 lists the overpotentials obtained via the CNM and FPM (η_{CNM} and η_{FPM}) for different single-atom catalysts, as well as the rate-determining steps. In both methods, the Co atoms exhibit stronger interactions with the intermediate species than the Ni atoms, regardless of the surrounding environment (the red curves in Fig. 3a are lower than those in Fig. 3b, and the red curves in Fig. 3c are lower than those in Fig. 3d). However, the overstrong interaction with intermediate species in Co@graphene is detrimental to its activity. As we can see, the overpotential for CoN_4@-graphene is lower than that for NiN_4@graphene, while the overpotential for Co@graphene is larger than that for Ni@graphene in both methods (CNM and FPM). Thus, the activity trends of Co vs. Ni are consistent between the two methods.

However, the rate-determining steps predicated by the CNM and FPM are different. In Co@graphene, for example, the fourth step is the rate-determining step in the CNM, while the FPM predicted that the third step is the rate-determining step. Meanwhile, the η_{CNM} and η_{FPM} of the same catalyst are different as well, and the difference can be as great as 0.48 V (NiN_4@graphene, for example, $\eta_{CNM} = 0.86V$ and $\eta_{FPM} = 1.34V$). The CoN_4@graphene has been predicted theoretically to be an excellent catalyst with a small overpotential calculated from the CNM [32,33]. Ref. [32] reports a 0.37-V overpotential, and Ref. [33]] reports a 0.38-V overpotential, agreeing with $\eta_{CNM} = 0.55V$ based on CNM calculations within the calculation uncertainties (e.g., magnetic movement and solvent model). However, there is a conspicuous lack of experimental evidence for its good catalytic properties. Our FPM result of $\eta_{CPM} = 0.85V$ indicates that this indeed might not be a good catalyst. On the other hand, the Ni@graphene is proven to be an excellent catalyst experimentally [13]. Both the CNM and FPM predict that the overpotential of Ni@graphene is low, 0.35 V and 0.39 V respectively. Thus, overall, we find that the FPM provides good agreement with experiments.

Fig. 4 plots the U-dependent energy ($\Delta G_{U_{electrode}} - \Delta G_{-4.4}$) for each intermediate state when $U_{electrode}$ shifts from −4.4 V to a lower potential. Here, for each intermediate state, Δ means it is

Table 1
The overpotential of OER on different single-atom catalysts calculated via the charge-neutral method, the fixed-potential method (V), and the fixed-charge method (FCM).

	CoN_4@graphene	Co@graphene	NiN_4@graphene	Ni@graphene
η_{CNM}	0.55(2)	1.01(4)	0.86(2)	0.35(3)
η_{FPM}	0.85(1)	0.73(3)	1.34(1)	0.39(2)
η_{FCM}	0.86(1)	0.67(3)	1.43(1)	0.41(2)

Note: The charge state of four intermediate species in the FCM (Q_{FCM}) is fixed at the average charge of the four intermediate states from the FPM calculation at $U^h_{electrode}$,as shown in Table S4 in the Supporting Information. The rate-determining step numbers are also listed in parentheses.

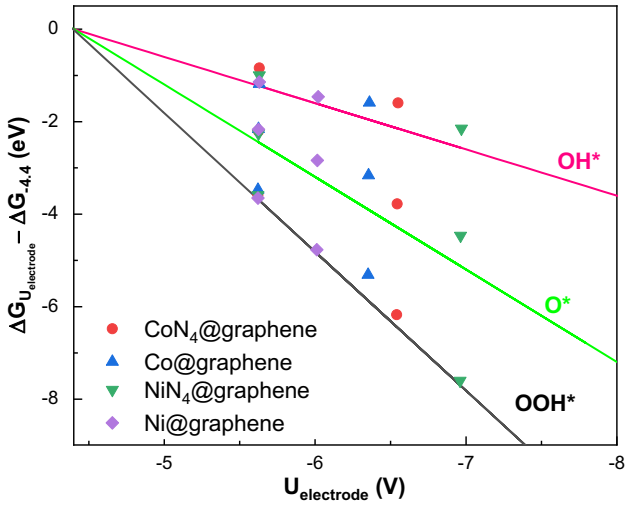

Fig. 4. The energy dependence (the electronic energy transfer from the electrode to a catalyst, $\Delta G_{U_{electrode}} - \Delta G_{-4.4}$) for each intermediate when $U_{electrode}$ ranges from −4.4 V to lower potential. The energy dependence for OH*, O*, and OOH* obtained by the charge-neutral method is plotted as a solid line, while that obtained by the fixed-potential method is plotted as symbols.

referenced from the corresponding * state. For the CNM, based on Eq. (2), these *U*-dependent energies for different intermediates state should be the straight lines plotted in Fig. 4 following the equation

$$\Delta G^{CNM} = \Delta G_{U_{electrode}} - \Delta G_{-4.4} = N_e \times (U_{electrode} + 4.4) \quad (6)$$

For OH*, O*, and OOH*, the N_e is 1, 2, and 3, respectively. The *U*-dependent energies in the FPM (ΔG^{FPM}) do not follow a simple expression. In Eq. (4), everything depends on the $U_{electrode}$. Nevertheless, they can be calculated directly, and have been plotted with scatters in Fig. 4. As we can see, the values for each intermediate species in different systems collapse into a single curve. Overall, the curves are close to the ideal $N_e \times (U_{anode} + 4.4)$ dependence as in the CNM case. For OH*, O*, and OOH*, the slope is slightly smaller than the ideal slope N_e (N_e = 1, 2, and 3 for OH*, O*, and OOH*, respectively). This slight reduction in slope might be a result of Le Chatelier's principle, which states that in a real system, under external perturbation (here the change of the potential $U_{electrode}$), the effects of the adjustment of the system will reduce the effect of this external perturbation (here this means to effectively reduce $U_{electrode}$ + 4.4, hence reducing the slope).

Overall, the collapse into a single curve (for every kind of intermediates in different systems), and the relative closeness to the ideal slope are a bit surprising. If one used only the ΔG_{elect}: $(1 + q2 - q1)eU_{electrode}$ to analyze the energy dependence on $U_{electrode}$, one could get a rather different result, as $q2 - q1$ is far from zero, and $q2$, and $q1$ also depend sensitively on $U_{electrode}$. In Fig. S1 in the Supporting Information, we show the effect of this term $(1 + q2 - q1)eU_{electrode}$ from the FPM calculation, compared with that of the $N_e \times (U_{electrode} + 4.4)$ term from the CNM calculation. As we can see, the result scatters in Fig. S1 in a disorderly fashion. However, when the ΔG_{chem} are added, the total U-dependent energies as shown in Fig. 4 are close to the CNM cases due to the compensation between ΔG_{chem} and ΔG_{elect}. That indicates that the CNM is not completely wrong. However, we believe the quantitative error in the free energies is not as important as the qualitative error in rate-determining steps. We will prove that the rate-determining steps obtained in the FPM can be confirmed via the fixed-charge method with proper charge rather than the charge-neutral state in the following.

We next use the Co—O bond in the CoN_4@graphene with OH* adsorbing as an example to illustrate how the M—O bond responds to the potential change. Fig. 5 plots the DOS of Co-*d* and O-*p* orbitals in the CoN_4@graphene with OH* adsorbing under different potentials. The orbitals of the Co—O bond are labeled by their electron clouds. As we can see, the Co—O bonds mainly consist of two compounds: σ bond (hybridization of Co-d_z^2 and O-p_z) and π bond (hybridization of Co-d_{yz} and O-p_y). The σ bond is stronger as the density state of the hybridization of Co-d_z^2 and O-p_z disperses from −8 to −4 eV, while the density state of the weaker π bond is very local. The contribution of the Co-d_{yz} orbital to the π bond decreases gradually as the applied potential shifts from −4.40 V to a lower energy level, −5.63 V, which weakens Co—O bond strength. When the $U_{electrode}$ shifts further to −6.55 V, the Co-d_{xy} orbital becomes empty. Meanwhile, the local magnetic moments of Co also jump from 0.58 V ($U_{electrode} = -5.63\ V$) to 1.55 V ($U_{electrode} = -6.55\ V$; see Table S6 in the Supporting Information). That indicates that the applied potential changes the Co—O bond substantially. Therefore, different electrode potentials will give different local electronic structures and binding environments, which change the catalytic activity and energy. Similar results are also observed in recent fixed-potential work by Liu and co-workers[10]. Therefore, the difference between CNM and FPM is mainly due to the active site's local electronic structure changes at different potential (or different total charge). Thus, one cannot use the local electronic structure at a neutral charge to describe the reaction at the operando electrode potential.

The compensation phenomenon between ΔG_{chem} and ΔG_{elect} indicates that the difference between FPM and CNM (e.g., for the overpotential difference) may not be caused only by noninteger charge transfers from one intermediate state to another intermediate state (from $q1$ to $q2$) while the potential is fixed. The total charge states that change the local electronic structure of catalysts may be the main factor that induced the overpotential difference from the traditional charge-neutral method. In other words, it does not matter whether it is a fixed-charge (canonical) or fixed-potential (grand canonical) calculation. What matters is the charge value to be fixed (not neutral charge). In the FPM case, to get the overpotential, it is clear the most relevant calculation is the one with $U_{electrode}$ equals to $U^h_{electrode}$. Thus, for the fixed-charge method (FCM), the issue is that we should have the calculation at the non-neutral charge (hence, not CNM) where the resulting Fermi energy is not far away from $U^h_{electrode}$. Instead, the charge value we used for FCM fits the average Fermi energy of the four intermediate states equal or close to $U^h_{electrode}$. One can consider this a self-consistent

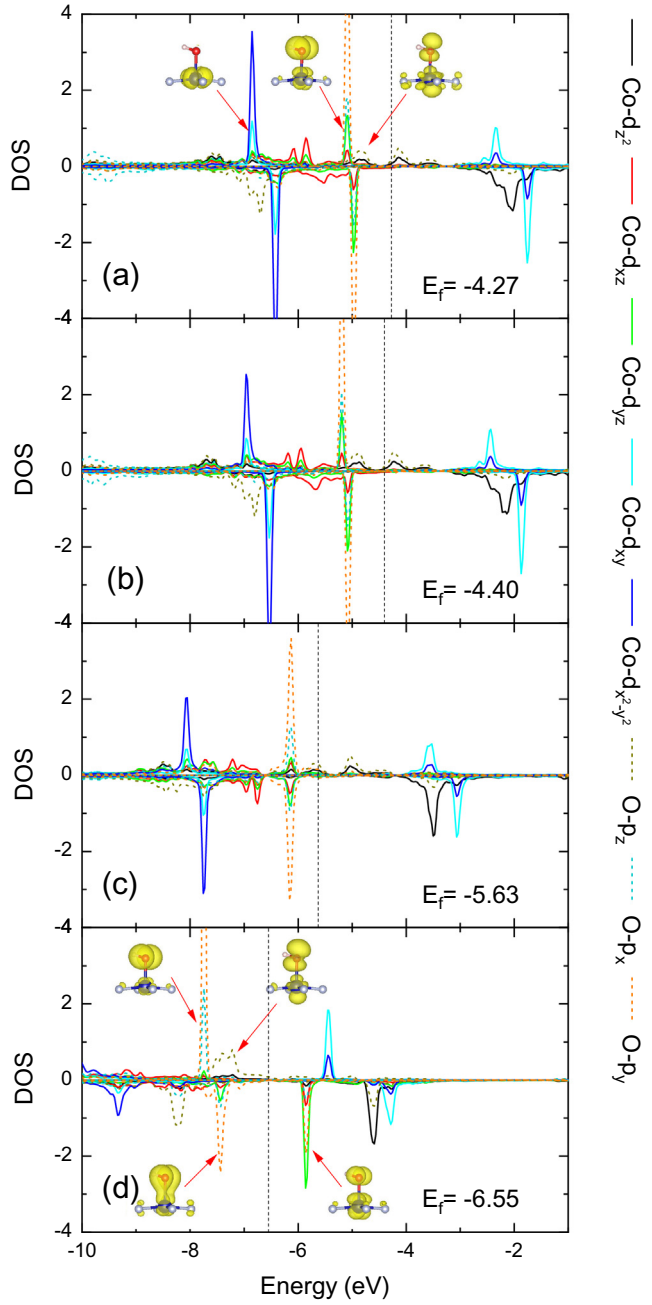

Fig. 5. The density of state of Co*d* and O*p* orbitals in the CoN_4@graphene with OH* adsorbing under different potentials.

procedure, since the $U^{h}_{electrode}$ value in this procedure will in turn depend on the charge value used in the FCM. Furthermore, if the average Fermi energy is close to the $U^{h}_{electrode}$, the final result will not so sensitively depend on the method we used any more (FCM or FPM). Guided by this assumption, we have calculated the FCM using the average charge of the four intermediate states from $U^{h}_{electrode}$ obtained by the FCM. The average charges used for the four systems (CoN_4@graphene, Co@graphene, NiN_4@graphene, and Ni@graphene) are + 2.15, +1.60, +2.53, and + 1.15, respectively (as listed in Table S4 in the Supporting Information). Equation (2) is used to calculate the Gibbs free energy, while G_{OH^*} and G_* are calculated with the above total charge state. The resulting energy curves atU^{h}_{anode} = -6.55, −6.36, −6.97, and −6.02 for the four systems are shown in Fig. 6, in comparison with the FPM at these potentials. We see that the corresponding curves are rather similar except for Co@graphene. The difference in Co@graphene is caused by the free energy of * obtained by the FCM being lower by about 0.3 eV than that obtained in the FPM. The overpotentials of the FCM from these curves are 0.86, 0.67, 1.43, and 0.41 V, as shown in Table 1, which agree very well with the FPM results. In addition, the rate-determining steps obtained via FCM and FPM are the same for all the systems. Note that it is also possible that this FCM could still be wrong if the charges from one intermediate state differed significantly from another intermediate state in the FPM calculation (Table S5 in the Supporting Information). Conversely, if the Fermi energies of the four intermediate states at the above FCM are very different, this FCM can also break down. In our case, these variations are relatively small; thus the FCM works fine. Therefore, the traditional NCM will cause errors in both rate-determining steps and overpotentials in the real operando local environments simulation. These issues can be improved via the FCM with proper charge. However, it is still a challenge to determine the charge state that should be used by these methods themselves.

4. Conclusions

In summary, we have used the fixed-potential grand canonical method to simulate the electric charging effects between an electrode and single-atom catalysts during OER processes at different electrode potentials. The FPM automatically adjusts the total system charge to satisfy an applied electrode potential. At this applied potential, the system can have dramatically different local orbital occupations at the catalytic site than in the neutral charge system, resulting in different microscopic environments for catalytic chemical reactions. The grand-canonical-FPM-calculated overpotential can differ from the traditional CNM results by as much as 0.48 V, and can also yield different rate-limiting steps. On the other hand, this difference is not really from the difference between fixed-potential or fixed-charge calculations (through the four steps), but from the local electronic configuration difference used to calculate the chemical reactions. This assumption is demonstrated by a test using the FCM calculation (the same charge for the four steps), but with the charge that yields the desired average Fermi energy corresponding to the operando applied electrode potential (instead of the neutral charge). This FCM calculation yields almost the same results as the FPM calculation. Therefore, the traditional NCM will cause errors in both rate-determining steps and overpotentials in the real operando local environments simulation. These issues can be improved via the FCM with proper charge values. However, it is still a challenge to determine the total charge value that should be used in the FCM. The fixed-potential method (grand canonical method), in which the total number of electrons in the system is floated automatically to match the given electrode Fermi energy, is a better model to simulate the electrochemical reactions in a more straightforward way. We believe our work advances the understanding of potential effects on the catalytic process in real electrochemical reactions and offers practical guidance for designing catalysts.

As analyzed in our study, the major difference between the FPM and the NCM comes from the occupation of the local density of state at different electrode potentials. This effect is probably strongest for 2D material due to its relatively low density of states. In the bulk electrode, even if the potential changes significantly relative to the vacuum level, the Fermi energy relative to the density of states in the bulk should not change. Nevertheless, for oxides such as TiO_2, $SrTiO_3$, and WO_3, the surface density of state occupations can still change significantly due to the existence of a surface density of states near the Fermi energy. As a result, there could still be a significant FPM effect. On the other hand, for metal, due to the

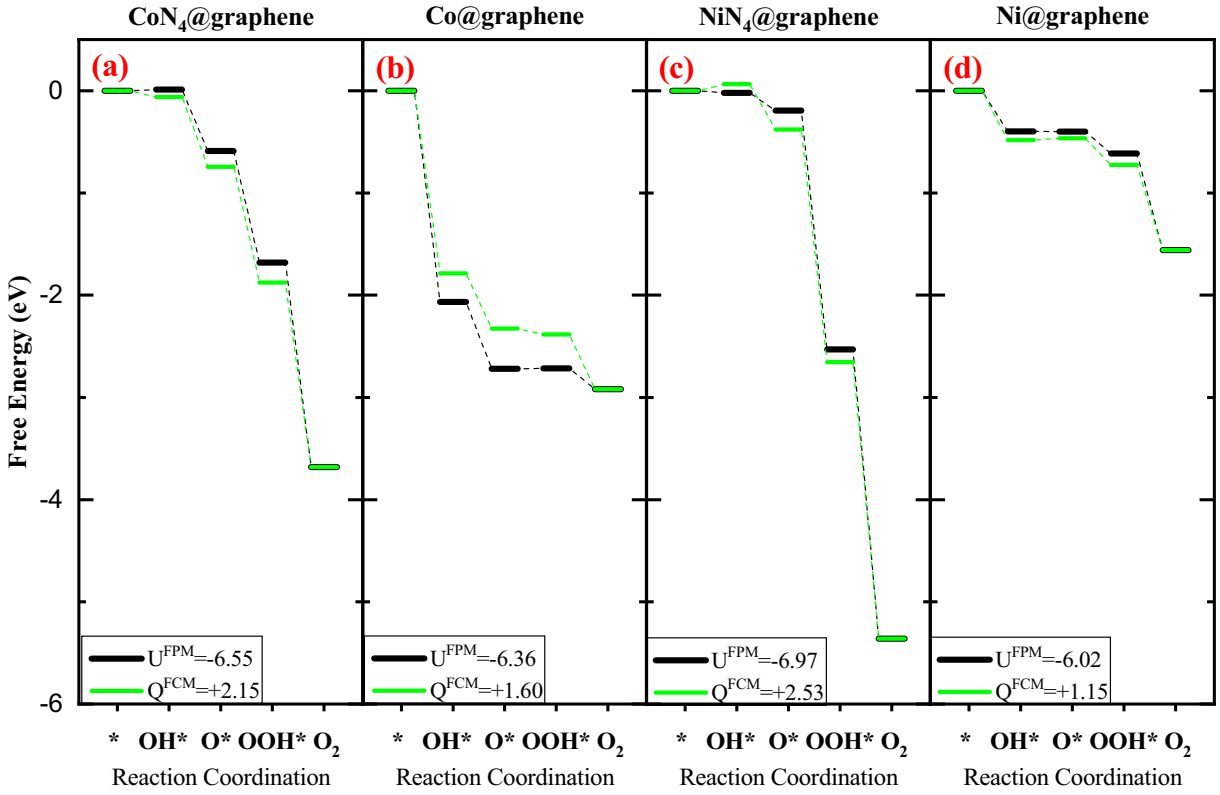

Fig. 6. The free energy diagrams for the oxygen evolution reaction on CoN_4@graphene(a), Co@graphene(b), NiN_4@graphene(c), and Ni@graphene(d). $U_{electrode}$ = -4.4 V is the ideal hydrogen evolution potential, while $U_{electrode}$ = -5.63 V is the ideal oxygen evolution potential. Q^{FCM} is the average charge of the four intermediate states from the FPM calculation at $U^{h}_{electrode}$(as listed in Table S4 in the Supporting Information).

high bulk density of states near the Fermi energy and the relatively simple electronic structure for the surface, the effect could be rather small. That said, there could be other effects, caused by the change of charge in the reaction species themselves, for example, during the energy barrier calculation, when the molecule has different structures. Such change is not related to the substrate, but the species themselves. Such effects can significantly alter the results for energy barrier calculations, and will be studied in the future.

The supporting information provides the following: A brief instruction to PWmat code, the solvent model, and the Poisson–Boltzmann equation. The process of OER for the charge-neutral method. The Fermi energy levels of different neutral catalysts and intermediates. The charge states of different catalysts and intermediates when the Fermi energy level is set to −4.4 eV and −5.63 V via the fixed-potential method. The charge states of different catalysts and intermediates when the Fermi energy level is set to U^{h}_{anode}(V) via the fixed-potential method, The Fermi energy levels of different catalysts and intermediates when the charge is set to the average charges at U^{h}_{anode}(V) via the fixed-charge method. The energy dependence obtained from the electron transfer energy term $(\Delta G^{elect}_{U_{anode}} - \Delta G^{elect}_{-4.40})$ for each intermediate when $U_{electrode}$ shifts from −4.4 V to lower potentials, and the total magnetic moment and local magnetic moment of Co in CoN_4@graphene with OH* adsorbing under different $U_{electrode}$ and neutral states.

Declaration of Competing Interest

The authors declare that they have no known competing financial interests or personal relationships that could have appeared to influence the work reported in this paper.

Acknowledgments

This work was supported by the Assistant Secretary for Energy Efficiency and Renewable Energy of the U.S. Department of Energy under the Battery Materials Research (BMR) program. The theoretical work in this research used the resources of the National Renewable Energy Laboratory High-Performance Computing.

Appendix A. Supplementary material

Supplementary data to this article can be found online at https://doi.org/10.1016/j.jcat.2020.08.032.

References

[1] G. Beni, L.M. Schiavone, J.L. Shay, W.C. Dautremont-Smith, B.S. Schneider, Electrocatalytic oxygen evolution on reactively sputtered electrochromic iridium oxide films, Nature 282 (1979) 281–283.
[2] Y. Meng, X. Zhang, W.-H. Hung, J. He, Y.-S. Tsai, Y. Kuang, M.J. Kenney, J.-J. Shyue, Y. Liu, K.H. Stone, X. Zheng, S.L. Suib, M.-C. Lin, Y. Liang, H. Dai, Highly active oxygen evolution integrated with efficient CO_2 to CO electroreduction, Proc. Natl. Acad. Sci. USA 116 (2019) 23915–23922.
[3] J.K. Nørskov, J. Rossmeisl, A. Logadottir, L. Lindqvist, J.R. Kitchin, T. Bligaard, H. Jónsson, Origin of the Overpotential for Oxygen Reduction at a Fuel-Cell Cathode, J. Phys. Chem. B 108 (2004) 17886–17892.
[4] Á. Valdés, Z.W. Qu, G.J. Kroes, J. Rossmeisl, J.K. Nørskov, Oxidation and Photo-Oxidation of Water on TiO2 Surface, J. Phys. Chem. C 112 (2008) 9872–9879.
[5] J. Long, S. Chen, Y. Zhang, C. Guo, X. Fu, D. Deng, J. Xiao, Direct Electrochemical Ammonia Synthesis from Nitric Oxide, Angew. Chem. Int. Ed. 59 (2020) 9711–9718.
[6] X. Liu, Y. Jiao, Y. Zheng, M. Jaroniec, S.-Z. Qiao, Building Up a Picture of the Electrocatalytic Nitrogen Reduction Activity of Transition Metal Single-Atom Catalysts, J. Am. Chem. Soc. 141 (2019) 9664–9672.
[7] K. Chan, J.K. Nørskov, Electrochemical Barriers Made Simple, J. Phys. Chem. Lett. 6 (2015) 2663–2668.
[8] J.-S. Filhol, M. Neurock, Elucidation of the Electrochemical Activation of Water over Pd by First Principles, Angew. Chem. Int. Ed. 45 (2006) 402–406.

[9] J.D. Goodpaster, A.T. Bell, M. Head-Gordon, Identification of Possible Pathways for C-C Bond Formation during Electrochemical Reduction of CO_2: New Theoretical Insights from an Improved Electrochemical Model, J. Phys. Chem. Lett. 7 (2016) 1471–1477.
[10] D. Kim, J. Shi, Y. Liu, Substantial Impact of Charge on Electrochemical Reactions of Two-Dimensional Materials, J. Am. Chem. Soc. 140 (2018) 9127–9131.
[11] S. Ravishankar, A.G.I. William, A.A. Tomas, Grand canonical electronic density-functional theory: Algorithms and applications to electrochemistry, J. Chem. Phys. 146 (2017) 114104.
[12] J. Guan, Z. Duan, F. Zhang, S.D. Kelly, R. Si, M. Dupuis, Q. Huang, J.Q. Chen, C. Tang, C. Li, Water oxidation on a mononuclear manganese heterogeneous catalyst, Nat. Catal. 1 (2018) 870–877.
[13] L. Zhang, Y. Jia, G. Gao, X. Yan, N. Chen, J. Chen, M.T. Soo, B. Wood, D. Yang, A. Du, X. Yao, Graphene Defects Trap Atomic Ni Species for Hydrogen and Oxygen Evolution Reactions, Chem 4 (2018) 285–297.
[14] H. Fei, J. Dong, Y. Feng, C.S. Allen, C. Wan, B. Volosskiy, M. Li, Z. Zhao, Y. Wang, H. Sun, P. An, W. Chen, Z. Guo, C. Lee, D. Chen, I. Shakir, M. Liu, T. Hu, Y. Li, A.I. Kirkland, X. Duan, Y. Huang, General synthesis and definitive structural identification of MN4C4 single-atom catalysts with tunable electrocatalytic activities, Nat. Catal. 1 (2018) 63–72.
[15] Y. Ouyang, L. Shi, X. Bai, Q. Li, J. Wang, Breaking scaling relations for efficient CO_2 electrochemical reduction through dual-atom catalysts, Chem. Sci. 11 (2020) 1807–1813.
[16] W. Liu, L. Zhang, W. Yan, X. Liu, X. Yang, S. Miao, W. Wang, A. Wang, T. Zhang, Single-atom dispersed Co–N–C catalyst: structure identification and performance for hydrogenative coupling of nitroarenes, Chem. Sci. 7 (2016) 5758–5764.
[17] Y. Wang, J. Mao, X. Meng, L. Yu, D. Deng, X. Bao, Catalysis with Two-Dimensional Materials Confining Single Atoms: Concept, Design, and Applications, Chem. Rev. 119 (2019) 1806–1854.
[18] G. Gao, E.R. Waclawik, A. Du, Computational screening of two-dimensional coordination polymers as efficient catalysts for oxygen evolution and reduction reaction, J. Catal. 352 (2017) 579–585.
[19] G. Gao, S. Bottle, A. Du, Understanding the activity and selectivity of single atom catalysts for hydrogen and oxygen evolution via ab initial study, Catal. Sci. Technol. 8 (2018) 996–1001.
[20] W. Jia, Z. Cao, L. Wang, J. Fu, X. Chi, W. Gao, L.-W. Wang, The analysis of a plane wave pseudopotential density functional theory code on a GPU machine, Comput. Phys. Commun. 184 (2013) 9–18.
[21] W. Jia, J. Fu, Z. Cao, L. Wang, X. Chi, W. Gao, L.-W. Wang, Fast plane wave density functional theory molecular dynamics calculations on multi-GPU machines, J. Comput. Phys. 251 (2013) 102–115.
[22] J.P. Perdew, K. Burke, M. Ernzerhof, Generalized Gradient Approximation Made Simple, Phys. Rev. Lett. 77 (1996) 3865–3868.
[23] J.P. Perdew, M. Ernzerhof, K. Burke, Rationale for mixing exact exchange with density functional approximations, J. Chem. Phys. 105 (1996) 9982–9985.
[24] S. Grimme, Semiempirical GGA-type density functional constructed with a long-range dispersion correction, J. Comput. Chem. 27 (2006) 1787–1799.
[25] X. Zhao, Y. Liu, Unveiling the Active Structure of Single Nickel Atom Catalysis: Critical Roles of Charge Capacity and Hydrogen Bonding, J. Am. Chem. Soc. 142 (2020) 5773–5777.
[26] S.L. Dudarev, G.A. Botton, S.Y. Savrasov, C.J. Humphreys, A.P. Sutton, Electron-energy-loss spectra and the structural stability of nickel oxide: An LSDA+U study, Phys. Rev. B 57 (1998) 1505–1509.
[27] Z. Wang, Y. Yang, D.L. Olmsted, M. Asta, B.B. Laird, Evaluation of the constant potential method in simulating electric double-layer capacitors, J. Chem. Phys. 141 (2014) 184102.
[28] K. Mathew, R. Sundararaman, K. Letchworth-Weaver, T.A. Arias, R.G. Hennig, Implicit solvation model for density-functional study of nanocrystal surfaces and reaction pathways, J. Chem. Phys. 140 (2014) 084106.
[29] G. Fisicaro, L. Genovese, O. Andreussi, N. Marzari, S. Goedecker, A generalized Poisson and Poisson-Boltzmann solver for electrostatic environments, J. Chem. Phys. 144 (2016) 014103.
[30] O. Andreussi, I. Dabo, N. Marzari, Revised self-consistent continuum solvation in electronic-structure calculations, J. Chem. Phys. 136 (2012) 064102.
[31] S. Trasatti, The absolute electrode potential: an explanatory note (Recommendations 1986), J. Electroanal. Chem. Interfac. Electrochem. 209 (1986) 417–428.
[32] H. Xu, D. Cheng, D. Cao, X.C. Zeng, A universal principle for a rational design of single-atom electrocatalysts, Nat. Catal. 1 (2018) 339–348.
[33] Y. Zhou, G. Gao, Y. Li, W. Chu, L.-W. Wang, Transition-metal single atoms in nitrogen-doped graphenes as efficient active centers for water splitting: a theoretical study, Phys. Chem. Chem. Phys. 21 (2019) 3024–3032.